Lab on a Chip

# Faster sperm selected by rheotaxis leads to superior early embryonic development in vitro



| | |
|---|---|
| Journal: | *Lab on a Chip* |
| Manuscript ID | LC-ART-08-2023-000737.R1 |
| Article Type: | Paper |
| Date Submitted by the Author: | 29-Oct-2023 |
| Complete List of Authors: | Yaghoobi, Mohammad; Cornell University,<br>Abdelhady, Abdallah; Cornell University College of Veterinary Medicine, Clinical Sciences<br>Favakeh, Amirhossein; Cornell University, Food Science<br>Xie, Philip; Weill Cornell Medicine, Reproductive Medicine; Weill Cornell Medicine<br>Cheung, Stephanie; Cornell University, The Ronald O. Perelman and Claudia Cohen Center for Reproductive Medicine<br>Mokhtare, Amir; Cornell University College of Agriculture and Life Sciences,<br>Lee, Yoke; Cornell University College of Veterinary Medicine, Clinical Sciences<br>Nguyen, Ann; Cornell University, Food Science<br>Palermo, Gianpiero; Weill Cornell Medicine<br>Rosenwaks, Zev; Cornell University<br>Cheong, Soon; Cornell University, Clinical Sciences<br>Abbaspourrad, Alireza; Cornell University, Food Science; Cornell University |
| | |

# Faster sperm selected by rheotaxis leads to superior early embryonic development in vitro

Mohammad Yaghoobi,[1] Abdallah Abdelhady,[2] Amirhossein Favakeh,[1] Philip Xie,[3] Stephanie Cheung,[3] Amir Mokhtare,[1] Yoke Lee Lee,[2] Ann V. Nguyen,[1] Gianpiero Palermo,[3] Zev Rosenwaks,[3] Soon Hon Cheong,[2] Alireza Abbaspourrad[1,*]

[1]Food Science Department, College of Agriculture and Life Sciences (CALS), Cornell University, Ithaca 14853, New York, USA.

[2]Department of Clinical Sciences, College of Veterinary Medicine (CVM), Cornell University, Ithaca 14853, New York, USA.

[3]The Ronald O. Perelman and Claudia Cohen Center for Reproductive Medicine, Weill Cornell Medicine, New York, NY 10021, USA.

* Corresponding Author: Alireza Abbaspourrad, E-mail: alireza@cornell.edu

## ABSTRACT

To understand the impact of sperm speed as they swim against the flow on fertilization rates, we created conditions similar to the female reproductive tract (FRT) on a microfluidic platform for sperm selection. Selected sperm were evaluated based on early development of fertilized embryos. Bovine and human spermatozoa were selected at various fluid flow rates within the device. We found that the speed of bovine spermatozoa increases as the flow rate

increases and that the amount of DNA fragmentation index is lowered by increasing the flow rate. Bovine spermatozoa selected by our platform at low (150 μL $h^{-1}$, shear rate 3 $s^{-1}$), medium (250 μL $h^{-1}$, shear rate 5 $s^{-1}$), and high flow rates (350 μL $h^{-1}$, shear rate 7 $s^{-1}$) were used for fertilization and compared to sperm sorted by centrifugation. The samples collected at the highest flow rate resulted in the formation of 23% more blastocysts compared to the control. While selecting for higher quality sperm by increasing the flow rate does result in lower sperm yield, quality improvement and yield may be balanced by better embryonic development.

**Keywords:** sperm speed; rheotaxis; embryo development

## INTRODUCTION

Since its development assisted reproductive technologies, like in vitro fertilization (IVF), have allowed millions of human couples to conceive[1] and increased the breeding efficiency of other mammalian species such as cattle.[2] Early studies of IVF were more focused on the oocyte to improve the outcomes, but it was quickly found that the chance of fertilization in rabbits and mice increased dramatically when oocytes were exposed to in vivo capacitated sperm.[3] Sperm sorting was found to have an important role on fertilization efficiency and has since become a crucial part of efforts to improve the IVF process.[4,5]

Traditionally, sorting is done by washing semen through several rounds of centrifugation.[6] However, centrifugation techniques have been reported to cause damage to sperm DNA.[7] They do not select sperm similar to how they are naturally selected in FRT.[8] Recently researchers started investigating microfluidic methods to sort spermatozoa and began introducing the resulting devices into clinical settings.[9] These early clinical trials showed that

sperm separation via microfluidics imposes less harmful effects on the sperm membrane integrity, mitochondrial activity, and morphology as well as reducing DFI.[5,6,9–11]

Much of the data about how spermatozoa find the oocyte in vivo, and the role of the FRT in the spermatozoa's journey, are controversial.[12,13] For instance, Miki and Clapham[12] argue that the fluid flow in FRT after coitus is sufficient for long-range sperm guidance. On the other hand, Hino and Yanagimachi[13] discuss the effect of active peristaltic contraction on the hydrodynamics of FRT contradicts any guiding mechanism for sperm finding the oocyte. Despite a lack of direct experimental evidence, many agree that the hydrodynamics, topology and chemical composition of the FRT place barriers in the spermatozoa's path.[4,14] Spermatozoa are equipped with multiple features to overcome these barriers, and the FRT and the sperm have co-evolved for ideal selection conditions.[15] Microfluidic devices have made it easier to study and select for sperm features by implementing gentle flows,[16,17] filter-like components,[18,19] and the possibility of automation.[20] These devices also include investigations of the four navigational mechanisms of sperm cells; thigmotaxis (swimming along boundaries), thermotaxis (swimming against the direction of a temperature gradient), chemotaxis (swimming against chemical gradients) and rheotaxis (swimming against the flow).[4] Chemotaxis and thermotaxis are short range mechanisms that guide sperm toward the egg in the oviduct and are only active in approximately 10% of the sperm population in mammalian species.[21–23] Although sperm chemotaxis in mammals remains controversial,[24,25] recent strides toward sorting spermatozoa based on chemotaxis and thermotaxis has led to higher quality spermatozoa in humans.[26]

Cells are attracted to the walls when swimming in confined spaces.[27] This hydrodynamic feature suggests that a significant amount of sperm motion takes place along the microenvironment walls within the FRT.[28] This feature is proposed to lead spermatozoa to the

fertilization site through the narrow crevices of the FRT[29] and could be used for selection of highly motile spermatozoa.[30,31] Aligned with this, studies on sperm sorting based on boundary-following characteristics showed improvement both in human and bovine spermatozoa in their motility parameters and DNA integrity.[32,33] Although the sorting time is reduced using these methods, the fertilization ability of the sperm samples was not tested.

The mucosal fluid of the FRT, other post-copulation secretions, and ciliary motion, generate a robust flow through the narrow lumen of the mammalian oviduct from ovaries to the uterus.[12] This fluid flow may guide or select sperm cells via rheotaxis.[12,34] Several microfluidic platforms have been designed to select spermatozoa based on rheotaxis using either a corral-based system or a platform with contraction and expansion channels to induce rheotaxis.[35,36] Other platforms contain a collection chamber and a loading reservoir connected to each other via a rheotaxis channel to obtain rheotactically capable spermatozoa.[10,37–39] These studies have explored sperm quality improvement via rheotaxis at one shear rate; the effect of modulating the shear rate has been recently reported,[40] but its implication on sperm selection and embryonic development is still not well understood. Also the sperm yield in all the rheotaxis based sperm separation platforms as compared to the input sample, still needs improvement.

Previously, we introduced the rheotaxis quality index (RHEOLEX) as a potential biomarker for fertility screening: the higher the number of spermatozoa with higher rheotaxis capacity, the higher the pregnancy outcomes.[41] We have now designed a microfluidic channel to separate motile spermatozoa based on their rheotaxis capability and then how spermatozoa selected at different flow rates impacts early embryonic development. We confirmed that the kinematic features of the separated spermatozoa (speed, beating amplitude and frequency) were tuned by the intensity of the flow rate. At higher flow rates only spermatozoa with high speed

were selected at the cost of the total number of sperm. The DNA integrity of the selected spermatozoa was evaluated. We selected ~2 million bovine spermatozoa and used these spermatozoa to perform chamber-based IVF. We then compared the development of embryos resulting from spermatozoa selected at various speeds with each other and with sperm sorted by centrifugation. Under optimum conditions, selecting spermatozoa at high flow rates resulted in 23 % improvement in blastocyst rate when compared to centrifugation-based sperm sorting.

# RESULTS

## Design layout and operation

To ensure that spermatozoa are guided upstream for rheotaxis-based sperm separation, the device was designed to have regions of high and low shear rates. We designed strictures, using triangular prisms in a microfluidic channel: a network of 3 rows of 42 parallel prisms (**Fig. 1A-C**). These strictures were inspired by the constrictions present in the uterotubal junction (UTJ) in the FRT of many mammalian species.[42] Curved veins around the triangular prisms and straight veins between each group of curved veins and prisms, were used to avoid trapping air bubbles while loading the device (**Fig. 1A**).[43] The main channel is 180 μm deep, while the cross section of the veins run the width of the device, they are only 40 μm deep and 80 μm wide such that they create a bump for the media and sperm to flow over and keep air bubbles from forming (**Fig. 1A and B**). The total device capacity is 80 μL of semen. We used 3 rows of strictures to increase the chance of spermatozoa being oriented upstream reducing sperm loss due to a reorientation lag. But increasing the number of rows more than that would reduce the capacity of the device.

The device is operated by loading the semen sample through the outlet and then washing the semen with media from the inlet, which sweeps the semen toward the outlet. Debris and

nonmotile spermatozoa are washed away with the media and sperm that are capable of rheotaxis remain in the device after washing. Spermatozoa have multiple opportunities to pass through the strictures and be guided upstream, provided they have enough strength to swim against the flow (**Fig. S1**).

To estimate the required time for the washing step, a computational fluid dynamics simulation for a 2-dimensional layout of our device was done by ignoring the guiding veins. The contours of the relative concentration of media in the chip at 210 s intervals for a flow rate of 300 μL $h^{-1}$ indicates that the media (red contours) washes the middle of the channel much faster than the regions near the walls (**Fig. 1D**). C represents semen, which enters the device at a concentration of $C_i$. C can vary between 0 (media) and $C_i$, therefore the ratio of $C/C_i$ varies between 0 and 1. We attribute this to a lower velocity of the fluid near the boundaries. Thus, nonmotile sperm and debris near the side walls will take longer to be washed.

Our simulation indicates that the volume fraction ($\phi$) of semen remaining in the chip decreases over time and with increasing flow rate (**Fig. 2A**). The time needed so that $\phi$ = 3, 5, 10 and 15% versus various flow rates is then calculated (**Fig. 2B**). The diagram of time required for washing flattens for higher flow rates and it exponentially increases for smaller flow rates. We chose the times for $\phi$ = 10% to ensure that theoretically 90% of debris and nonmotile spermatozoa would be discharged. Otherwise, to reach 95% removal ($\phi$ = 5%), the washing time nearly doubles that of $\phi$ = 10%. Increasing the washing time beyond this does not help with cleaning the sample and it over-exposes the spermatozoa to additional shear which might have harmful effects.

While washing, the motile spermatozoa trajectories are affected by the presence of the prisms. Spermatozoa starting either from the right-side within the stricture, or outside of the

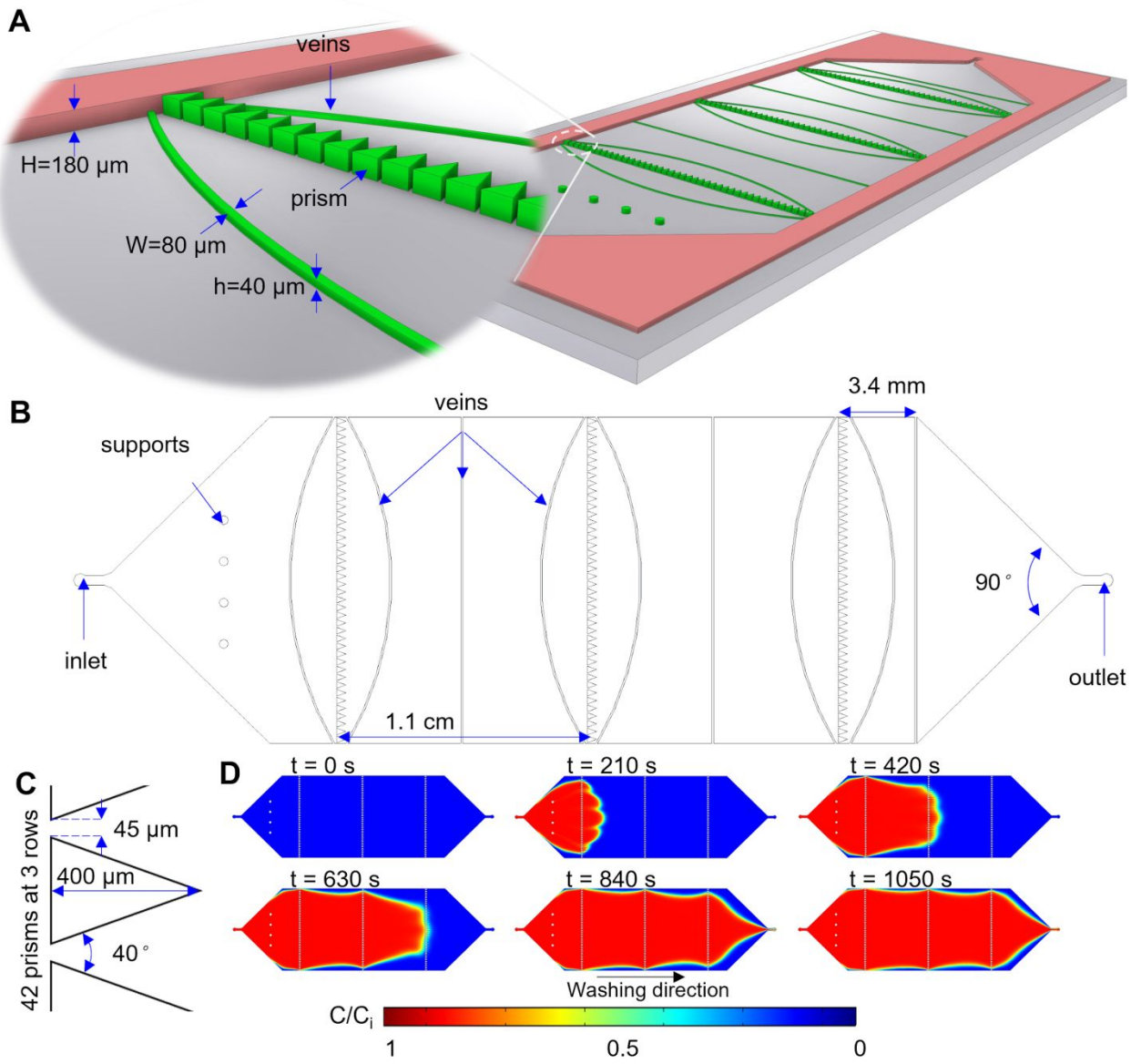


**Fig. 1** (A) perspective view of the device with the inset showing the dimensions of the loading veins and prisms. (B) The distance between the rows is 1.1 cm and the inlet and outlets are connected with 90° fans. The inlet area has 4 supports of 200 μm diameter. (C) The dimensions of the prisms. (D) After semen is loaded, the medium (red, $C_i$) is injected from the inlet at various flow rates and the simulation results show how the medium washes the semen (blue).

139 stricture, swim to the left side of the stricture against the flow (**Fig. 2C**). The shear rate contours

140 on the xy-plane near the top wall and the xz-plane in the middle of the stricture show that right at

141 the point of the strictures the shear rate is zero. However, near the top or the bottom walls (z = 18

μm, shown in **Fig. 2D**), and 20 μm before and after the strictures, the shear rate is high enough (3 $s^{-1}$) to cause the spermatozoa to reorient upstream.[35,44] The reason that the shear rate at the strictures is zero is that the velocity profile is flat in the middle plane at the strictures due to symmetry (**Fig. S2**). Therefore, if the spermatozoa are moving near the left side of the prism and enter the stricture, they are dragged downstream, but once they reach the space between two prisms, they can reorient upstream.

The average shear rate ($\gamma$) at the stricture, the red line at z = 18 μm (**Fig. 2D**), linearly changes as a function of the flow rate (**Fig. 2E)** so that shear rate ($s^{-1}$) = 0.02 (h $\mu L^{-1}$ $s^{-1}$) × flow rate (μL $h^{-1}$). Our results are expressed in terms of change in shear rate, as opposed to flow rate, as shear rate allows for cross comparison of results if, for example, the depth of the device is increased to accommodate a higher volume of semen. Expressing the results in terms of flow rate would introduce inconsistencies in the resulting rheotaxis information since flow rate varies by volume.

**Accumulation of sperm at the strictures**

Human and bovine spermatozoa undergo rheotaxis between shear rates of approximately 3 to 10 $s^{-1}$. We confirmed this range by quantifying the number of human spermatozoa that accumulate at the strictures within the shear rate range of 2 to 46 $s^{-1}$ (**Fig. 3A**). We focused the microscope at one of the strictures and monitored the human sperm rheotaxis at various shear rates. To quantify the sperm accumulation in the strictures, we have used the algorithm we

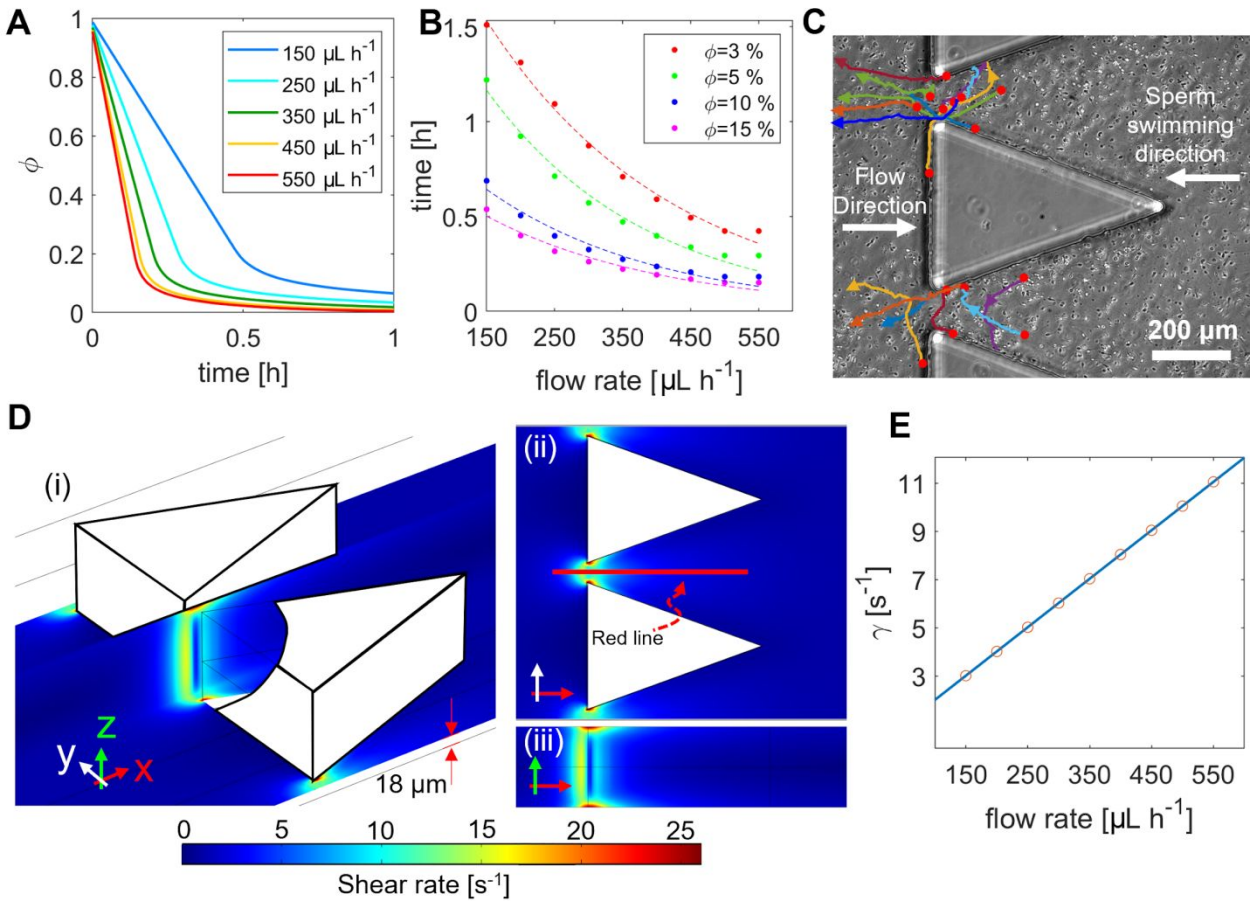


**Fig. 2** (A) $\phi$ over time decreases faster for higher flow rates. The rate of semen discharge decreases since the fluid velocity near the walls is low. (B) The time required for the washing steps is estimated numerically at various flow rates. The washing can stop when $\phi$ is 3, 5, 10 or 15 %. (C) as the semen is washed from the chip, the motile sperm with high DNA integrity and higher velocity would swim against the flow and are guided by the strictures through the rheotaxis mechanism to the inlet area and the lesser motile spermatozoa and debris would discharge from the outlet. (D) The shear rate contours in isometric projection (i), on the xy plane at z = 18 µm (ii) and xz-plane at the middle of the stricture (iii). One of the prisms is cut to assist visualization. (E) Average shear rate versus flow rate in the device.

161 developed for RHEOLEX.[42] This algorithm calculates the changes in pixel intensity for

162 consecutive frames and obtains the average intensity for 200 images to generate signal contours

163 (**Fig. 3A**). The signal is then averaged vertically for each shear rate along the x-axis after

164 eliminating the prisms from the image (**Fig. 3B**).

At low shear rates (2 $s^{-1}$) we found no accumulation since the shear rate is not sufficient to induce rheotaxis (**Fig. 3D**). This is consistent with the reported minimum shear rate for rheotaxis of bovine spermatozoa, 3 $s^{-1}$.[35] We found that for human spermatozoa, the RHEOLEX signal reaches a maximum at 9.2 $s^{-1}$ and decreases as the shear rate increases. The maximum signal intensity occurs at a distance from stricture (x) indicating that higher shear rates drag the spermatozoa downstream. The signal decreases to 0.3 at x/L = 0.6, where x is the distance from the contraction point between two prisms and L is the total length of the prism from contraction point to full expansion point. Although these images were taken from only two strictures in the middle row of the device, the velocity profile and shear rate in all of the strictures is the same except for along the boundaries (**Fig. S3**).

Using a one-dimensional convective transport of active particles we confirmed the accumulation of spermatozoa at the stricture. We found that the accumulation of spermatozoa at the strictures can be simulated numerically only by tracking the direction of the spermatozoa's motion and their location in a similar stricture geometry (**Fig. S5**). Previously, bacterial accumulation at similar contraction-expansion geometries have been studied using another one-dimensional approach.[45]

Spermatozoa accumulate at the strictures under medium shear rates in the range of 3 - 11 $s^{-1}$. At shear rates greater than 11 $s^{-1}$, the increased fluid velocity prevents spermatozoa from undergoing rheotaxis. While faster, stronger spermatozoa may stay in place at higher shear rates, the mechanical shear of the fluid at higher flow rates could cause damage. Therefore, sperm motility parameters determined by computer assisted sperm analysis (CASA), and other semen parameters such as DFI, and membrane integrity were used to evaluate selected sperm quality.

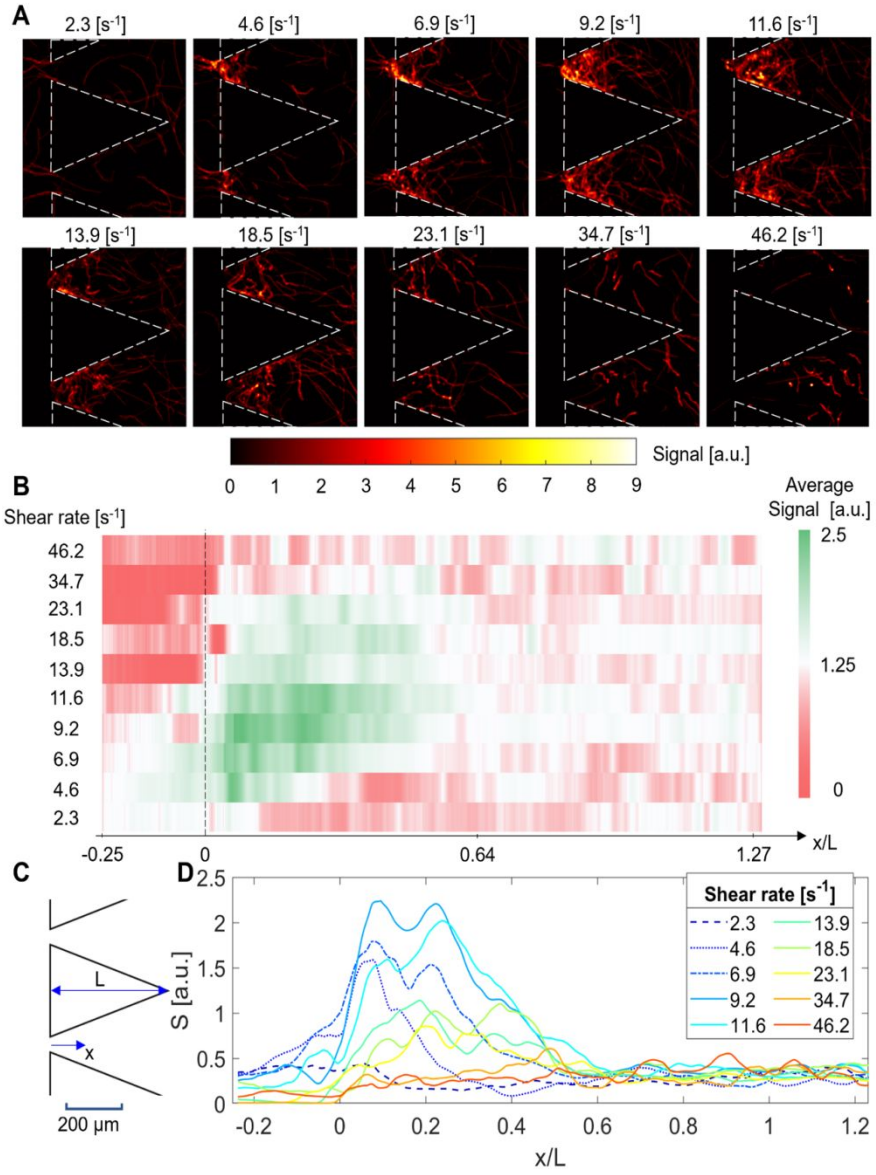


**Fig. 3** Accumulation of spermatozoa at the stricture at various shear rates. (A) As the shear rate increases the signal (S [a.u.]) increases and then decreases at higher shear rates, peaking at shear rate 9.2 $s^{-1}$. (**B**) The rheotactic sperm population at the stricture moves downstream because of the increase in the drag forces; the maximum of the mean signal S shifts to higher x values (distance from contraction point between prisms). (C) X values start at zero at the smallest distance between prisms. Minus x values indicate the region in front of the stricture. (D) Shows the moving average of the signal. The signal before and after stricture is close to zero and peaks at 0-200 µm and it reduces for shear rates greater than 10 $s^{-1}$.

For human spermatozoa, semen parameters were evaluated including sperm concentration, motility, normal morphology, and sperm chromatin fragmentation (SCF).

**Characterization of separated human spermatozoa**

Human semen analysis was carried out manually on a raw sample. Semen parameters were also accessed on selected spermatozoa isolated at various shear rates as well as conventional density gradient centrifugation (DGC)-processed spermatozoa. To further characterize the performance of our device, we calculated the sperm retrieval efficiency (RE).

A comparison was made between the same semen parameters among raw sample, DGC and rheotaxis selection (**Table 1**). Morphology and motility increased, whereas concentration and SCF decreased, indicating that significantly superior spermatozoa resulted from rheotaxis-based selection but at the cost of concentration.

**Table 1.** Comparison of the selected sperm quality with that of raw sample and DGC.

| | Raw | DGC | Overall selected spermatozoa | P value* |
|---|---|---|---|---|
| Concentration (M $mL^{-1}$) | 76.7 ± 33.4 | 49.9 ± 25.5 | 4.5 ± 4.7 | <0.0001 |
| Motility (%) | 45.5 ± 0.9 | 91.1 ± 1.1 | 96.3 ± 2.5 | <0.0001 |
| Morphology (%) | 3.2 ± 0.4 | 3.2 ± 0.4 | 4.0 ± 0.6 | <0.0001 |
| SCF (%) | 9.4 ± 2.0 | 8.1 ± 3.6 | 4.5 ± 2.1 | <0.001 |

*DGC vs selected spermatozoa (overall), paired t-test

In subanalysis, **Table 2** shows the sperm parameters with respect to shear rate. The concentration decreased with increasing the shear rate while motility increased and then decreased. RE was 42% at the maximum that occurred at a shear rate 5 $s^{-1}$ which is far more than the current rheotaxis-based sperm separation methods and minimum SCF was achieved at the same shear rate. Very similar to bovine spermatozoa, there is an optimum shear rate but since

human sperm swims slower than bovine sperm, the optimum shear rate is also lower. Morphology did not show any changes with various shear rates. (**Table S1** has additional details about data shown in **Table 2**.)

**Table 2.** Clinical quality parameters of rheotaxis-based human sperm selected at various shear rates.

| Shear rate (flow rate) | 3 $s^{-1}$ (150 µL $h^{-1}$) | 5 $s^{-1}$ (250 µL $h^{-1}$) | 7 $s^{-1}$ (350 µL $h^{-1}$) | 9 $s^{-1}$ (450 µL $h^{-1}$) | P value* |
|---|---|---|---|---|---|
| Concentration (M $mL^{-1}$) | 3.0 ± 3.1 | 5.6 ± 3.9 | 3.7 ± 1.8 | 2.7 ± 2.4 | <0.01 |
| Motility (%) | 94.7 ± 1.2 | 97.0 ± 2.2 | 97.2 ± 2.3 | 95.6 ± 3.3 | <0.05 |
| RE (%) | 28.3 ± 6.3 | 42.0 ± 6.0 | 30.2 ± 4.2 | 24.0 ± 4.3 | <0.001 |
| Morphology (%) | 3.8 ± 0.4 | 4.3 ± 0.6 | 4.3 ± 0.7 | 3.8 ± 0.7 | n.s. |
| SCF (%) | 4.6 ± 1.1 | 2.9 ± 0.6 | 3.7 ± 1.8 | 5.7 ± 2.5 | <0.001 |

*ANOVA, comparison between shear rate 5 $s^{-1}$ and 3 $s^{-1}$

In an additional analysis, we compared the proportion of X- and Y-bearing spermatozoa in relation to varying shear rates. Sperm cells possess a slightly different mass, depending on their gonosomal component. It is well-documented that the Y chromosome is smaller[46] and, as such, would have a lower mass than the X; therefore, we expected Y-bearing spermatozoa to possess a higher velocity and agility to perform rheotaxis. As the selection shear rate increased from 3 to 9 $s^{-1}$, we observed a gradual skew towards a greater proportion of Y-bearing spermatozoa (2-3%) (**Table 3**). These findings suggest that implementation of considerably higher shear rates may further skew a sperm population towards those carrying a Y chromosome. Although linear regression of the Y chromosome percentage and F-test showed no statistical significance (p-value = 0.1282 > 0.05, **Fig. S6**), this data is from limited samples and observations with a marginal difference. We believe that more experiments are needed to confirm sex bias of the swimming velocity of Y-bearing spermatozoa.

**Table 3.** Fluorescent in situ hybridization (FISH) results in human sperm separation for two patients.

| Sample ID | Patient | X % | Y % |
|---|---|---|---|
| Raw Semen | 1 | 52 | 48 |
| 3 $s^{-1}$ | 1 | 52 | 48 |
| 5 $s^{-1}$ | 1 | 51 | 49 |
| 7 $s^{-1}$ | 1 | 52 | 48 |
| 9 $s^{-1}$ | 1 | 51 | 49 |
| Raw Semen | 2 | 51 | 49 |
| 3 $s^{-1}$ | 2 | 51 | 49 |
| 5 $s^{-1}$ | 2 | 49 | 51 |
| 7 $s^{-1}$ | 2 | 49 | 51 |
| 9 $s^{-1}$ | 2 | 48 | 52 |

**Characterization of the separated bovine spermatozoa**

Sperm quality varies with separation conditions. We used CASA and DFI parameters to evaluate quality. We evaluated three types of bovine samples: raw semen; spermatozoa sorted via centrifugation (IVF control group); and spermatozoa selected in our microfluidic platform. We considered the results of the control and raw as categorical variables, but since the shear rate is a continuous variable a regression model was fitted to the data to show the trend. The minimum shear rate for rheotaxis behavior is greater than 3 $s^{-1}$, therefore, we chose the optimum sorting conditions for bovine spermatozoa to be within the shear rate range of 3 to 11 $s^{-1}$.

In CASA the head centroid is tracked and based on the head trajectory an averaged path is calculated. The velocity of the spermatozoa moving along this averaged path is called

averaged-path velocity (VAP). The faster the speed of the spermatozoa the higher the VAP would be. VAP shifted to higher velocities as the shear rate increased but reached a maximum value. We confirmed this trend in bovine spermatozoa by CASA for more than 150 sperm cells randomly tracked from among the hundreds of thousands of spermatozoa selected using our microfluidic device (**Fig. S4**). However, the control group showed a wide range of VAP distributions and had no significant differences with VAP at any of our shear rates or that of raw sample.

The total motility percentage of the samples increased as the shear rate increased up to 7 $s^{-1}$, then decreased at higher shear rates as the concentration of sorted samples drops below 5% of the initial sample (**Fig. 4B and D**). With the concentration of the sorted sample and the motility percentage from CASA. RE was roughly 40% for $\gamma = 3\ s^{-1}$ and 5 $s^{-1}$, but RE decreased to 28% for 7 $s^{-1}$ (**Fig. S7**). As expected from our calculations, the overall RE decreased as the washing flow rate increased. Total sperm count also significantly decreases by increasing shear rate from 1.72 million at shear rate 3 $s^{-1}$ to 0.31 million at shear rate 5 $s^{-1}$ (**Table S2**).

The deviation of the sperm head centroid from its averaged path is called amplitude of lateral head displacement (ALH); at higher amplitudes of beating, ALH is higher. In our experiments ALH decreased as the shear rate increased up to 7 $s^{-1}$ and increased thereafter. There is not a significant difference between ALH of the control and raw samples.

And finally, the frequency by which the head trajectory crosses the averaged path determines beat cross frequency (BCF). In theory, BCF and ALH are inverse to each other with respect to shear rate and our results follow this pattern (**Fig. 4C, E**). Further, the BCF of the control significantly increased over that of the raw sample.

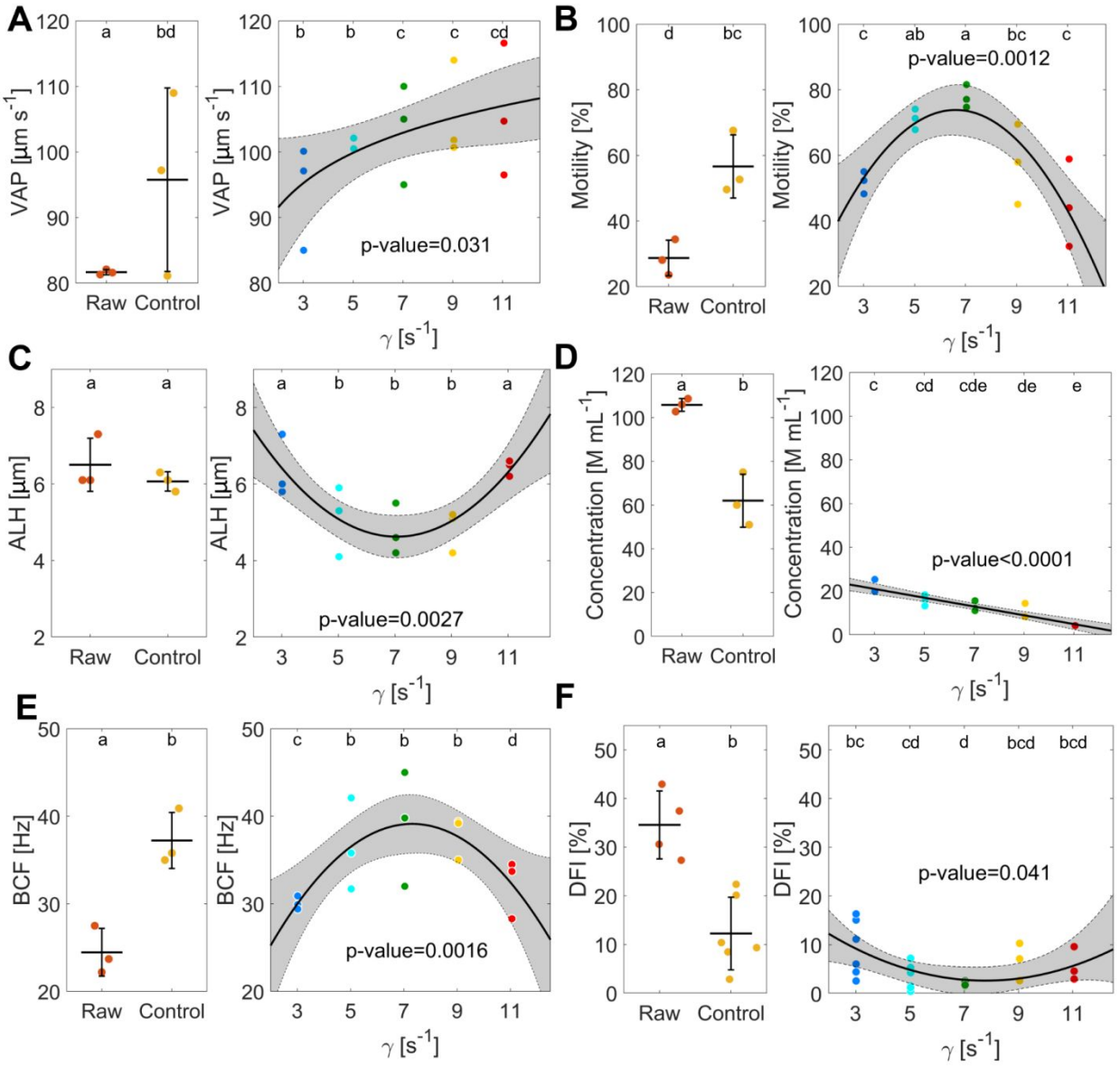


**Fig. 4** Computer assisted sperm analysis (CASA) parameters and DNA fragmentation index (DFI) of the separated spermatozoa in comparison to raw semen and centrifugation sorting. (A) VAP. (B) Motility percentage. (C) Amplitude of lateral head displacement (ALH). (D) Concentration of spermatozoa. (E) Beat cross frequency (BCF). and (F) DFI. * $p < 0.05$, ** $p < 0.01$ and $n \geq 3$. Shaded areas show the 95% confidence intervals. The statistical significance of each group is represented by connecting letter on top of each group. Groups with no common letters are significantly different. Paired t-test was used to compare means.

VAP, motility, ALH and BCF are only characteristics of sperm movement. After the fusion of a spermatozoon and an oocyte, the zygote checks the genome by its correction

mechanism. If spermatozoa carry a break in its DNA, embryonic development comes to a halt until the break is repaired which delays the growth. DNA breaks are quantified by DFI. For all sorted samples, DFI is lower than raw semen, with a minimum DFI found for samples selected at $\gamma = 7\ s^{-1}$ which is equivalent to the maximum and minimums of ALH, BCF, and motility.

In general, all of the quality assessments point to higher quality for both the control (centrifuged) and the spermatozoa selected based on rheotaxis over raw sample. Also, in selected spermatozoa, ALH, BCF and motility exhibit optimum values at $\gamma = 7\ s^{-1}$. **(Table S3** has the fitted lines for Fig. 4.)

**Bovine IVF procedure and embryonic development**

After sperm sorting, conventional IVF was performed using spermatozoa sorted via centrifugation (control) and spermatozoa separated by our microfluidic platform at shear rates of $3\ s^{-1}$, $5\ s^{-1}$ and $7\ s^{-1}$. As the shear rate increased, fewer spermatozoa are able to swim against the flow, therefore, the concentration of the selected spermatozoa decreased significantly as the shear rate increased (**Fig. 5B**). For the control, the method is adjusted so that the concentration of sorted semen is closer to the raw sample.

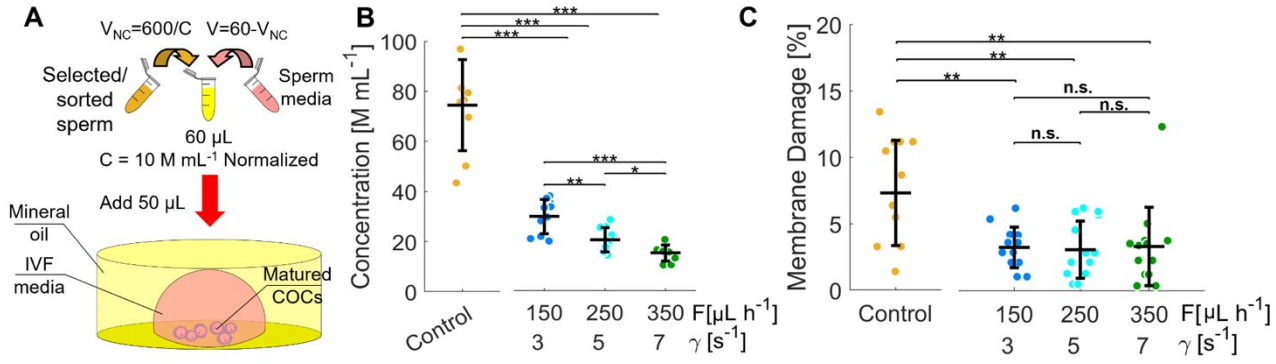


**Fig. 5** Conventional IVF process using various shear rates and centrifugation-based sperm separation as control. (A) Spermatozoa sorted using the microfluidic device and the centrifugation-based semen sorted are evaluated using NucleoCounter device for their concentration or C. $V_{NC}$=600/C microliter of the selected/sorted sperm and 60 – $V_{NC}$ microliter of media are mixed to produce samples of normalized concentration of 10 M mL$^{-1}$. (B) Concentration of sorted semen; as the shear rate increases the concentration of separated spermatozoa decreases. (C) Proportion of sperm with membrane damage is reduces for rheotaxis-based separation in comparison to centrifugation, * $p < 0.05$, ** $p < 0.01$, *** $p < 0.001$.

The concentration of samples was measured using a NucleoCounter cell counter. The concentration of insemination dose was normalized by dilution of the sperm samples with warm media to 10 M mL$^{-1}$. A volume of $V_{NC}$=600/C µL of selected/sorted sample, where C is the concentration of spermatozoa determined using the NucleoCounter, was added to 60 – $V_{NC}$ µL of media to produce 60 µL of samples with concentration of 10 M mL$^{-1}$. Normalized concentration samples were prepared for each group and 50 µL of the normalized sample was added to the chamber containing mature cumulus oocyte complexes (COCs) (**Fig. 5A**). Normalization is necessary because we wanted to see only the effect of shear rate on the cleavage and blastocyst rates.

We assessed the quality of the device separated spermatozoa by measuring the plasma membrane integrity. An intact plasma membrane will be able to keep non-membrane permeable

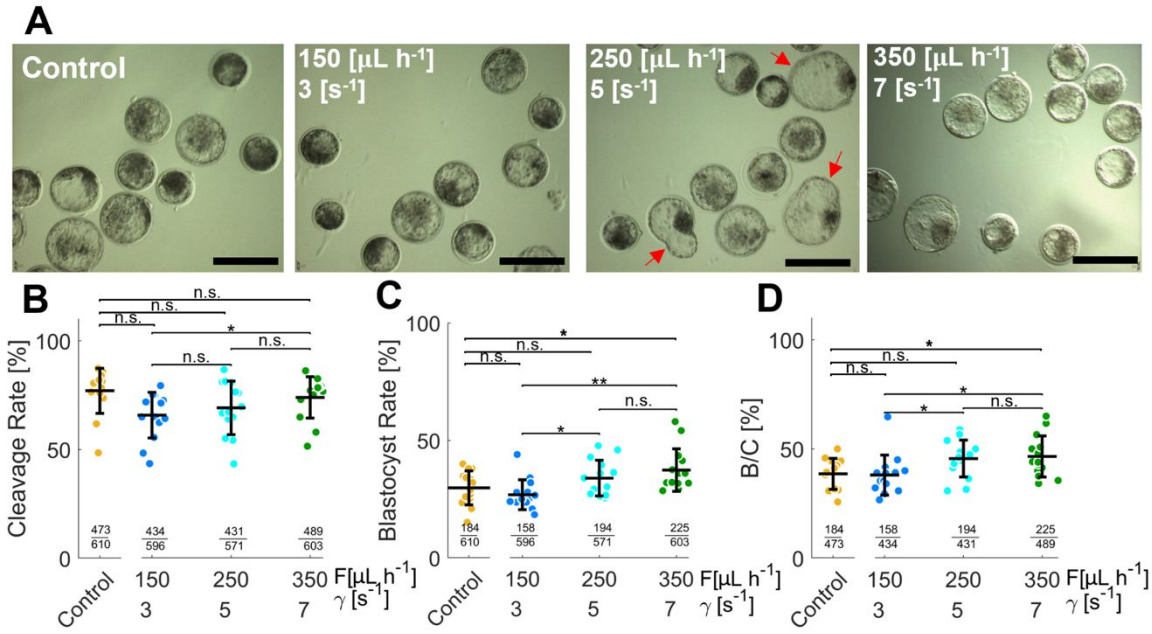


**Fig. 6** (A) The blastocysts for various groups. The red arrow shows hatched embryos. The scale bar is 200 µm. (B) Cleavage rate is approximately 80% for all the four groups; no statistical significance (n.s.). The fraction at each group shows the total number of cleaved embryos over total inseminated COCs. (C) As the shear rate increases, blastocyst rate increases while there is no significant difference between control and 3 and 5 $s^{-1}$ groups. At $\gamma = 7\ s^{-1}$, blastocyst rate increases to 37 % in comparison to 30 % of the control. The ratio shows the total number of blastocysts over total number of COCs. (D) Ratio of blastocysts over cleavage. * $p < 0.05$, ** $p < 0.01$.

stains, such as propidium iodide, out of the cell; whereas, in spermatozoa with damaged plasma membrane the stain will permeate the cell and stain the DNA in the nucleus. Some of the spermatozoa in raw semen may already have damage to their membrane reducing their success in the following IVF; thus, finding a method that effectively removes the damaged cells is important to successful IVF outcomes. . We found that for our device, the membrane damage was slightly decreased by about 4 % in comparison to the control (**Fig. 5C**). There was no significant difference between shear rates and membrane damage, leaving out the effect of mechanical shear on the integrity of the plasma membrane.

The embryos produced through IVF for spermatozoa separated at $\gamma = 3\ s^{-1}$ and the control were smaller than those of spermatozoa separated at higher shear rates. At higher shear rates the embryos often included hatched or larger size embryos (**Fig. 6A**). There is no significant difference between the cleavage rate in control and any of the microfluidic-based sorting (**Fig. 6B**). The blastocyst rate, however, showed a significant difference between the control and spermatozoa separated at $\gamma = 7\ s^{-1}$; as the shear rate increases, the blastocyst rate also increases (**Fig. 6C and D**). This trend seems to reach a plateau as no significant difference between the blastocyst rate of 5 $s^{-1}$ and 7 $s^{-1}$ is observed, while there is a significant difference between shear rates of 3 $s^{-1}$ and 5 $s^{-1}$ and also between 3 $s^{-1}$ and 7 $s^{-1}$.

## DISCUSSION

Previously we developed a method of characterizing mammalian sperm rheotaxis and concluded that spermatozoa from bulls with higher fertilization rates show higher rheotaxis ability.[41] Here, we postulated that sorting spermatozoa with higher rheotaxis capability could result in better fertilization outcomes in IVF cycles. To test this, we designed and characterized a high throughput microfluidic platform to separate spermatozoa with various rheotaxis abilities within a network of parallel strictures. The semen was loaded into the chip followed by media at different flow rates. The media swept away both debris and low motility spermatozoa. The spermatozoa that were capable of rheotaxis remained in the chip. By tuning the flow rate, thus tuning the shear rate in the device, rheotactically competent spermatozoa were separated. The spermatozoa, selected based on various shear rates, were then used in IVF to assess their fertilization ability.

Previous researchers have shown that a minimum shear rate is required for rheotaxis in both human and bovine sperm.[44] In our microfluidic platform we found that at shear rates below 3 $s^{-1}$, there was no accumulation of spermatozoa at the stricture. As the shear rate increases, rheotaxis is induced and spermatozoa are oriented upstream once they are in the shear zone of the stricture (the open triangle space between the prisms). If the free-swimming velocity of the spermatozoa is higher than the fluid velocity at the stricture, the spermatozoa surpass the fluid drag force and moves upstream (**Fig. 3B and D**). This will cause faster sperm locomotion to be redirected toward the inlet area and lead to their accumulation over time (**Movie S1**). This redirection does not occur without fluid flow; defying the ratchet effect[27] due to prisms' shape in guiding the spermatozoa to the inlet.

At areas farther from the stricture, $x > L$ or $x < 0$ (**Fig. 3C**), the velocity and the shear rate decrease and the spermatozoa follow their free-swimming motion again. Sperm accumulation occurs at $x = 0$; the highest signal intensity is observed at vicinity of $x = 0^+$ at shear rates between 3 $s^{-1}$ to 11 $s^{-1}$ (**Fig. 3A**). However, as the shear rate increases, the drag force on the spermatozoa increases and the maximum peak of the signal sweeps downstream to the point that the signal intensity barely spikes. But the near zero intensity of sperm signals at $x < 0$ for shear rates of higher than 11 $s^{-1}$ is an indication that spermatozoa cannot pass the barrier under these conditions. So, it is best to perform separation at shear rates 3 to 11 $s^{-1}$.

The CASA parameters and the DFI of the separated bovine spermatozoa showed the best sperm quality at $\gamma = 7\ s^{-1}$. That is, sperm speed becomes flat at $\gamma = 7\ s^{-1}$, DFI reached a minimum of 3% at this shear rate and ALH and BCF showed their minimum and maximum respectively. In comparison, human spermatozoa swims at lower speeds and our analysis of human sperm SCF showed that optimum quality occurs at $\gamma = 5\ s^{-1}$. Although the concentration of sorted

spermatozoa declines with higher shear rate and VAP increases, the motility percentage reaches a maximum at $\gamma = 7\ s^{-1}$. The increase in motility is due to the washing effect, but the decrease in motility for shear rate more than $7\ s^{-1}$ is attributed to the dilution effect.[47] We observed that as the seminal fluid content becomes diluted in the media, the spermatozoa's affinity for the CASA chamber walls increased; this resulted in sperm head tethering to the walls and many motile spermatozoa were counted as nonmotile. However, those spermatozoa that did not stick to the walls, had higher VAP. Single VAP distributions versus shear rate (**Fig. S4**) had a bimodal distribution: one peak about 50 $\mu m\ s^{-1}$ and the other at 135 $\mu m\ s^{-1}$. This distribution resembled a combination of raw sample's VAP and that of selected sample. As the shear rate increases the intensity of the first peak weakens and that of the second peak becomes stronger. This is due to the spermatozoa that linger near the side walls that are not swept away as effectively as the spermatozoa in the middle of the channel at lower $\gamma$ (**Fig. 1D)**.

At $\gamma = 7\ s^{-1}$, the ALH is at a minimum and the BCF is at its maximum. Nagata et al. showed that there are two types of sperm movement pattern in their rheotaxis sorted spermatozoa; transitional sinuous (TS) where sperm head sways laterally while moving forward, and progressive non-sinuous (PN) where sperm head stays on average trajectory while moving forward.[10] TS features larger ALH and lower BCF and VAP compared to the PN type. Our data indicate that as the shear rate increases from 3 to $7\ s^{-1}$ sorted spermatozoa shifts from TS to PN (**Fig. 4C and E**). The lateral movement exhibited by TS motion would allow the head of the spermatozoa to be exposed to the higher fluid velocity in the center of the stricture and be swept downstream, whereas spermatozoa exhibiting PN would remain closer to the wall and experience lower flow.

Nagata et al. also reported higher incidence of artificial insemination (AI)-related pregnancies in the case of TS type movement rather than PN.[10] This seems to be in contradiction to our IVF results which indicate as the shear rate increased, associated with PN type movement, the blastocyst rate increased significantly. However, since Nagata et al. performed AI, the FRT may play an important role in sperm selection whereas in our experiments, spermatozoa meet the oocytes directly. Also, In AI, the PN spermatozoa might undergo untimely hyperactivation before reaching the oocyte (transition to TS) and lose the chance of successful fertilization. However, in IVF, the activation of oocytes and the spermatozoa exposure to the capacitation media is controlled. Also, none of our separation experiments took more than two hours; less than required time for sperm capacitation.[48]

Up to the $\gamma = 7\ s^{-1}$ the DFI decreased, however beyond $7s^{-1}$, there was a slight increase in DFI (although not statistically significant). The lack of damage to the plasma membrane means that the reduced DFI at higher shear rates is likely due to apoptosis in nonmotile sperm cells present in the selected sample (**Fig. 5D**). The trend of no change in membrane damage versus shear rate rules out the effect of shear damage causing the increase in DFI for shear rates more than $7\ s^{-1}$. Therefore, the increase in DFI could be explained by a high level of reactive oxygen species (ROS) available in the sperm cells with higher velocities.[9] Thus, the spermatozoa separated at very high shear rates could have higher DFI.

The fertilization rates of various groups showed no change except for $3\ s^{-1}$ and $7\ s^{-1}$ which is merely due to the very high motility of the $7\ s^{-1}$ group despite the lower DFI of the spermatozoa at $7\ s^{-1}$. As long as the motility of spermatozoa is not impaired, fertilization rates have been shown to be independent of high DFI because the paternal genome does not participate in the early stages of embryo development.[49] Blastocyst formation, however, is

affected by DNA fragmented spermatozoa because at this stage the paternal genome is involved. We attribute the higher blastocyst rate of group 7 $s^{-1}$ with respect to the others to the lower DFI in the selected sample and not merely the motility percentage because the insemination dose was maximized at 10,000 spermatozoa per COC. Further, the motility of the group 5 $s^{-1}$ is lower than the group 7 $s^{-1}$ and yet the blastocyst rate does not vary significantly. We also observed higher incidence of hatching and larger embryos within the group 7 $s^{-1}$ indicating a higher developmental rate. This higher rate could, in part, be attributed to oocyte's DFI correction mechanism in group 5 $s^{-1}$ which delays the development rate and also optimizes the level of ROS in the fertilizing sperm which possibly regulates the metabolism of resulting embryos. Further experiments must be planned to characterize this observation and distinguish the underlying mechanisms.

Based on the results presented here, we can conclude that our platform is a very efficient and suitable method of sperm separation in bovine and human based on rheotaxis since it resulted in less DNA damage and higher speed. We found the optimum of the performance of the device to be around shear rate of 7 $s^{-1}$ for bovine and 5 $s^{-1}$ for human spermatozoa. Further, by performing IVF cycles for nearly 2400 oocytes we confirmed that as we select for higher rheotaxis ability in selected spermatozoa, the fertilization increases accordingly.

Since the concentration of sorted semen can be low for low motility samples, this method might not be optimal in the cases of male infertility due to low sperm counts or low motility, however, it can be useful in conventional IVF of non-male factors. Further, the idea of parallel strictures can be extended to higher capacity devices to accommodate low concentration samples to select the most competitive spermatozoa for the ICSI process.

# MATERIALS AND METHODS

## Device fabrication

Standard photolithography was used for fabrication of the mold.[50] The mold consisted of two layers. For the first layer SU-8 2100 was poured on silicon wafers (University Wafer) and spun at 3500 rpm for 30 s and baked for 5 and 35 min over 65 °C and 95 °C, respectively. We exposed the basked masks to 365 nm UV light through the laser-printed patterns mask for 30 s and subsequently baked on 95 °C for 15 min to create the 140 μm layer. The second layer was fabricated using SU-8 2025 by spinning at 3000 rpm for 30 s and exposure time of 20 s to add a 40 μm layer with corresponding patterns. The two layers were submerged in SU8-Developer for 30 min before hard-baking.

## Device loading and sperm collection

The device should be loaded from the outlet with media (BO-Semen Prep) with the flow rate of 3,000 μL $h^{-1}$ for 70 μL and then the flow rate reduced to 350 μL $h^{-1}$ for the area with the supports to reduce air entrapment. Overall, it takes 3 min to load each device with media. This loading media contained 0.2 % bovine serum albumin (BSA) to avoid tethering the sperm head to the glass and PDMS walls. After this 120 μL of semen was injected from the inlet via a pipette to replace the media and fill the device with semen. This step should be done quickly in order to avoid semen dilution (**Fig. S1**). After the washing step, the remaining sample was collected by setting the pipette on 80 μL and aspirating the sample from the inlet.

## Numerical simulation of washing step

COMSOL multiphysics software 5.4a was used to solve the coupled fluid velocity and pressure as well as transport of diluted species utilizing the finite element method.

$$\rho(u \cdot \nabla)u = -\nabla p + \mu\nabla \cdot (\nabla u + \nabla u^T) \quad (1)$$

$$\rho \nabla \cdot u = 0 \quad (2)$$

$$\frac{\partial C}{\partial t} + u \cdot \nabla C = D \nabla^2 C \quad (3)$$

where C is the local concentration of semen in the chip, u is the fluid velocity vector, and p is the pressure. μ = 1 mPa and D = $10^{-9}$ $m^2$ $s^{-1}$ are viscosity and diffusion coefficient, respectively. For the calculation of the volume fraction of semen in the chip ($\phi$) the following formula was used.

$$\phi = H \cdot \oint_{chip\ area} C\ dA \quad (4)$$

where dA is the element of the surface in the integral and H is the depth of the device.

**Human sperm morphology and motility**

Semen samples were incubated in 37 ℃ for 15 min to allow liquefaction. Semen analysis was performed manually in a Makler® counting chamber according to WHO manual.[51] Sperm concentration, motility, and morphology were evaluated on raw, DGC-processed (according to WHO manual),[51] and rheotactically selected spermatozoa.

**Computer assisted sperm analysis**

Motility, concentration, progressive motility, VSL, VCL, VAP, STL, LIN, ALH, BCF parameters were measured using the CASA system, Hamilton Thorn, ltd. A minimum of 150 spermatozoa were measured and for the samples of very low concentrations 100 spermatozoa were measured.

**Sperm DNA and chromatin integrity**

Acridine orange (AO) test was used for assessment of bovine sperm DNA integrity as described elsewhere[41] and TUNEL assay was used to evaluate SCF following the previous report.[11]

**Sperm membrane integrity**

Total sperm concentration in the sample was determined by NucleoCounter SP-100 (ChemoMetic) by stripping cell membranes with a detergent S-100 which allows the propidium iodide which is a non-membrane permeable DNA stain to stain the nucleus of spermatozoa. The number of sperm nuclei are counted, and the concentration determined by multiplying the number of sperm nuclei by the volume and dilution factor to determine the proportion of membrane damaged sperm, a second sample was prepared with the sperm sample diluted in media with no detergent. The difference between the total sperm concentration and the concentration of cells with membrane damage was the concentration of cells with the intact plasma membrane.

**Sperm samples**

Bovine sperm samples were purchased from Genex corporation (Ithaca, NY, USA) from a single fertile bull. Human semen from 7 men were collected by masturbation following a 2 to 5 d period of abstinence. Patients gave informed written consent to participate (IRB 0712009553). Only specimens with normal semen parameters (based on WHO guidelines [51]) were used for the experiments.

**Measurement of RE**

Knowing the average motility of the raw sample, and concentration and motility of the sorted samples, RE is calculated using the following formula:

$$RE\ \% = \frac{(M_{selected} \times C_{selected})}{(M_{raw} \times C_{raw})} \times 100 \qquad (5)$$

Here M denotes motility percentage and C refers to the total concentration. The subscript sorted and Raw refer to the type of the samples. With this information, the RE of various groups are calculated for 3 replicates.

**Theoretical modeling of sperm accumulation**

We have simplified our model to one dimensional motion of noninteracting spermatozoa using the Langevin equation:

$$\frac{dX_i}{dt} = V_f - V_{S_i} cos(\theta_i) \quad (6)$$

in which $X_i$, $\theta_i$ and $Vs_i$ are sperm position, direction of motion, and intrinsic velocity, respectively and subscript i indicates i-th sperm. $V_f$ is the velocity of the fluid which is a function of x which denotes the x location. For the effect of rheotaxis on the directional change of the sperm motion we used the following equation:[52]

$$\frac{d\theta_i}{dt} = -A\gamma sin(\theta_i) + \sqrt{2D_\theta}\,\chi \quad (7)$$

In the first term on the right-hand side of the equation, A and γ in the above equation are a constant and the shear rate respectively. If shear rate is between 11 $s^{-1}$ and 3 $s^{-1}$ this turning dynamics term is applied, otherwise it is ignored.[35] In the second term, $\chi$ is Gaussian noise with unit variance and mean zero which makes half of the spermatozoa right-turning and the other half left turning[53] and $D_\theta$is the rotational diffusion coefficient taken as 0.01 $rad^2\ s^{-1}$.[52] $\gamma = \frac{V_f}{W}$ and W is the width of the channel. From the continuity equation, $V_f$ can be calculated from the flow rate in the channel; meaning $V_f = \frac{Q}{W}$ in which Q is the flow rate.

**Oocytes collection and IVM**

Cow ovaries were collected from a local slaughterhouse. The ovaries were washed several times in a sterile saline. COCs were aspirated from follicles (2–8 mm in diameter) using an 18-gauge needle attached to an aspiration unit aspirating at a flow rate of 22.5-25 mL $H_2O$ $min^{-1}$. COCs with dark homogenous cytoplasm and at least 2 intact layers of cumulus cells were selected and

matured in IVM media (BO-IVM *IVF Bioscience, 61002)* as 50 COCs per each well containing 700 µL of the media covered with mineral oil and were incubated at 38.5 °C for 22 h in a humidified atmosphere of 5 v/v % $CO_2$ in air.

**IVF of bovine**

*Sperm preparation*: Frozen semen (from fertility-proven bulls) was thawed by immersing the straw in warm water (37 °C) for 20 s. For the control group, Spermatozoa were washed by centrifugation (350*g* for 5 min) in BO-Semen Prep (*IVF Bioscience, 61004)* as media. After removing the supernatant, the pellet was diluted with 1 mL of BO-Semen prep and centrifuged again for 5 min at 350*g*.

The microfluidic-based spermatozoa is sorted at shear rates of 3 $s^{-1}$, 5 $s^{-1}$ and 7 $s^{-1}$. The device was loaded with media. The media was replaced with 100 µL of the raw sample and then a syringe pump was used to generate 150, 250 and 350 µL $h^{-1}$ flow rates of media to wash the semen inside the chip for 35, 25 and 20 min respectively. These experiments were run in parallel. For the flow rates of 450 and 550 µL $h^{-1}$ which we used for sperm characterization experiments, the washing time was set at 18 and 17 min, respectively. Then the wasted semen from the outlet was discarded, and the tube from the syringe pump was detached from the inlet port, and the sorted sample was aspirated from the inlet port using a 200 µL pipette.

The inseminating dose for fertilization of each group was calculated using the Nucleo-counter then volume was adjusted to be 50 µL for each group via formulation demonstrated in **Fig. 5A**. Fifty (50) matured COCs were washed twice in 100 µL BO-IVF (IVF Bioscience, 61003) then transferred to a well so that the final content of the well is 450 µL of BO-IVF (IVF Bioscience, 61003) containing 50 COCs. Then the previously adjusted inseminating dose was added to the wells so that the total volume in each well is 500 µL overlaid with mineral oil.

Fertilization was carried out for 18 h at 38.5 °C in a humidified atmosphere of 5 v/v % $CO_2$ in air.

*IVC*: After fertilization, cumulus cells were removed by vortexing at maximum speed for 30 seconds to denude the zygotes. Presumptive zygotes were transferred to a 5-well plate containing 500 µL BO-IVC (*IVF Bioscience, 61001),* overlaid with mineral oil as 50 embryos per well. Embryos were then cultured in a humidified atmosphere of 5 % $O_2$, 5 % $CO_2$, and 90 % $N_2$ at 38.5 °C for 7 d.

*Assessment of cleavage and blastocyst rate*: Cleavage rate was assessed on day 2 of fertilization and blastocyst rate was assessed on day 7.

**Fluorescent in situ hybridization (FISH) analysis**

In preparation for FISH, slides were fixed in Carnoy's fixative (3:1 methanol:acetic acid) at room temperature (25 ℃) for 15 min, then placed on a slide moat at 37 °C overnight. Sperm decondensation was achieved by immersing the slides in 10 mmol/L dithiothreitol (DTT; Sigma Chemical Co., St. Louis, MO, USA) in 100 mmol $L^{-1}$ tris(hydroxymethyl) aminomethane (Trizma HCl; Sigma Chemical Co.). Slides were then washed for 1 min in 2x standard saline citrate (SSC; Vysis, Downers Grove, IL, USA), followed by hybridization with fluorescent probes. Sperm nuclei were counterstained by administering 7 µL of 4',6-diamino-2-phenylindole (DAPI; Abbott Molecular, Des Plaines, IL, USA) to each slide, which were then cover-slipped and assessed on a fluorescent microscope (Olympus BX61; New York/New Jersey Scientific, NJ, USA) at 1,000x. A minimum of 1,000 cells per slide were assessed to determine the ratio of X:Y spermatozoa (Applied Imaging, CytoVision v3.93.2).

**Statistical analysis**

JMP 16.0 software was used to perform the statistical analysis for bovine sperm characterization. For continuous variables analysis of variance was employed with either linear model or polynomial regressions and 5% was chosen for statistical significance as the result of F-test. For the categorical variables t-test was used with 5% as the significance level. For human sperm experimentations, paired t-test was performed to compare DGC and rheotactically selected spermatozoa with 5% as significance level. ANOVA test was performed to compare semen parameters among samples selected by each shear rate with significance at 5%. To further check the power with the significance level of 0.05 in our data we measured the common standard deviation as 5 %, considering 11 replicates the 5% increase in the blastocyst rate at $\gamma = 7\ s^{-1}$ in comparison to the control group the sample size is valid with the power of 70 % using T statistics.

## ASSOCIATED CONTENT

The supporting information includes additional supporting figures and data, and a movie.

## AUTHOR INFORMATION

**Corresponding Author**

Alireza Abbaspourrad - Food Science Department, College of Agriculture and Life Sciences (CALS), Cornell University, Ithaca 14853, New York, USA; Email: alireza@cornell.edu

**Authors**

Mohammad Yaghoobi - Food Science Department, College of Agriculture and Life Sciences (CALS), Cornell University, Ithaca 14853, New York, USA

Abdallah Abdelhady - Department of Clinical Sciences, College of Veterinary Medicine (CVM), Cornell University, Ithaca 14853, New York, USA

Amirhossein Favakeh - Food Science Department, College of Agriculture and Life Sciences (CALS), Cornell University, Ithaca 14853, New York, USA

Philip Xie - The Ronald O. Perelman and Claudia Cohen Center for Reproductive Medicine, Weill Cornell Medicine, New York, NY 10021, USA

Stephanie Cheung - The Ronald O. Perelman and Claudia Cohen Center for Reproductive Medicine, Weill Cornell Medicine, New York, NY 10021, USA

Amir Mokhtare - Food Science Department, College of Agriculture and Life Sciences (CALS), Cornell University, Ithaca 14853, New York, USA

Yoke Lee Lee - Department of Clinical Sciences, College of Veterinary Medicine (CVM), Cornell University, Ithaca 14853, New York, USA

Ann V. Nguyen - Food Science Department, College of Agriculture and Life Sciences (CALS), Cornell University, Ithaca 14853, New York, USA

Gianpiero Palermo - The Ronald O. Perelman and Claudia Cohen Center for Reproductive Medicine, Weill Cornell Medicine, New York, NY 10021, USA

Zev Rosenwaks - The Ronald O. Perelman and Claudia Cohen Center for Reproductive Medicine, Weill Cornell Medicine, New York, NY 10021, USA

Soon Hon Cheong - The Ronald O. Perelman and Claudia Cohen Center for Reproductive Medicine, Weill Cornell Medicine, New York, NY 10021, USA

**Author Contributions**

**M. Yaghoobi**: conceived and designed the experiments, performed the experiments, analyzed the data, wrote first draft and edited and reviewed later drafts; **A. Abdelhady**: conceived and designed the experiments, reviewed and edited manuscript; **A. Favakeh**: conceived and designed

the experiments, performed the experiments, reviewed and edited manuscript; **P. Xie**: conceived and designed the experiments, performed the experiments, reviewed and edited manuscript; **S. Cheung:** performed the experiments, wrote the paper, reviewed and edited manuscript; **A. Mokhtare**: conceived the experiments, reviewed and edited manuscript; **Y. L. Lee**: performed the experiments; review and edited manuscript; **A. V. Nguyen**: analyzed the data, reviewed and edited manuscript; **G. Palermo**: conceived and designed the experiments, analyzed the data, contributed materials/analysis tools, reviewed and edited manuscript; **Z. Rosenwaks**: contributed materials/analysis tools, reviewed and edited manuscript; **S. H. Cheong**: conceived and designed the experiments, analyzed the data, contributed materials/analysis tools, reviewed and edited manuscript; **A. Abbaspourrad:** conceived and designed the experiments, analyzed the data, contributed materials/analysis tools, reviewed and edited manuscript.

## ACKNOWLEDGEMENTS

We would like to express our gratitude toward Dr. Luis Henrique de Aguiar for preparation of the requirements for the IVF experiments in Cheong lab, and Dr. Kelley Donaghy for helping us to proof-read and edit the manuscript. This work was performed in part at the Cornell NanoScale Facility, a member of the National Nanotechnology Coordinated Infrastructure (NNCI), which is supported by the National Science Foundation (Grant NNCI-2025233). This study was approved by the Institutional Review Board of New York Presbyterian Hospital-Weill Cornell Medicine (IRB # 0712009553).

## REFERENCES

1. S. Franklin, *Reprod. Biomed. Online*, 2013, **27**, 747–755.

2. P. J. Hansen, *Theriogenology*, 2006, **65**, 119–125.

3. B. D. Bavister, *Reproduction*, 2002, **124**, 181–196.

4 . E. T. Leung, C.-L. Lee, X. Tian, K. K. Lam, R. H. Li, E. H. Ng, W. S. Yeung and P. C. Chiu, *Nat. Rev. Urol.*, 2021, 1–21.

5. R. Nosrati, P. J. Graham, B. Zhang, J. Riordon, A. Lagunov, T. G. Hannam, C. Escobedo, K. Jarvi and D. Sinton, *Nat. Rev. Urol.*, 2017, **14**, 707.

6. M. Muratori, N. Tarozzi, F. Carpentiero, S. Danti, F. M. Perrone, M. Cambi, A. Casini, C. Azzari, L. Boni and M. Maggi, *Sci. Rep.*, 2019, **9**, 7492.

7. J. G. Alvarez, J. L. Lasso, L. Blasco, R. C. Nuñez, S. Heyner, P. P. Caballero and B. T. Storey, *Hum. Reprod.*, 1993, **8**, 1087–1092.

8. D. Sakkas, M. Ramalingam, N. Garrido and C. L. Barratt, *Hum. Reprod. Update*, 2015, **21**, 711–726.

9. W. Asghar, V. Velasco, J. L. Kingsley, M. S. Shoukat, H. Shafiee, R. M. Anchan, G. L. Mutter, E. Tüzel and U. Demirci, *Adv. Healthc. Mater.*, 2014, **3**, 1671–1679.

10. M. P. B. Nagata, K. Endo, K. Ogata, K. Yamanaka, J. Egashira, N. Katafuchi, T. Yamanouchi, H. Matsuda, Y. Goto and M. Sakatani, *Proc. Natl. Acad. Sci.*, 2018, **115**, E3087–E3096.

11. A. Parrella, D. Keating, S. Cheung, P. Xie, J. D. Stewart, Z. Rosenwaks and G. D. Palermo, *J. Assist. Reprod. Genet.*, 2019, **36**, 2057–2066.

12 . K. Miki and D. E. Clapham, *Curr. Biol.*, 2013, **23**, 443–452.

13. T. Hino and R. Yanagimachi, *Biol. Reprod.*, 2019, **101**, 40–49.

14. S. S. Suarez, *Exp. Mech.*, 2010, **50**, 1267–1274.

15 . C.-K. Tung and S. S. Suarez, *Cells*, 2021, **10**, 1297.

16. C. Tung, L. Hu, A. G. Fiore, F. Ardon, D. G. Hickman, R. O. Gilbert, S. S. Suarez and M. Wu, *Proc. Natl. Acad. Sci.*, 2015, **112**, 5431–5436.

17. D. Seo, Y. Agca, Z. C. Feng and J. K. Critser, *Microfluid. Nanofluidics*, 2007, **3**, 561–570.

18. T. Chinnasamy, J. L. Kingsley, F. Inci, P. J. Turek, M. P. Rosen, B. Behr, E. Tüzel and U. Demirci, *Adv. Sci.*, 2018, **5**, 1700531.

19 . S. S. Suarez and M. Wu, *MHR Basic Sci. Reprod. Med.*, 2017, **23**, 227–234.

20. A. Mokhtare, B. Davaji, P. Xie, M. Yaghoobi, Z. Rosenwaks, A. Lal, G. Palermo and A. Abbaspourrad, *Lab. Chip*, 2022, **22**, 777–792.

21. Y. Yan, B. Zhang, Q. Fu, J. Wu and R. Liu, *Lab. Chip*, 2021, **21**, 310–318.

22. L. Xie, R. Ma, C. Han, K. Su, Q. Zhang, T. Qiu, L. Wang, G. Huang, J. Qiao and J. Wang, *Clin. Chem.*, 2010, **56**, 1270–1278.

23. S. Koyama, D. Amarie, H. A. Soini, M. V. Novotny and S. C. Jacobson, *Anal. Chem.*, 2006, **78**, 3354–3359.

24. H. Chang, B. J. Kim, Y. S. Kim, S. S. Suarez and M. Wu, *PloS One*.

25. M. Eisenbach and L. C. Giojalas, *Nat. Rev. Mol. Cell Biol.*, 2006, **7**, 276–285.

26. M. R. Doostabadi, E. Mangoli, L. D. Marvast, F. Dehghanpour, B. Maleki, H. Torkashvand and A. R. Talebi, *Andrologia*, 2022, e14623.

27. V. Kantsler, J. Dunkel, M. Polin and R. E. Goldstein, *Proc. Natl. Acad. Sci.*, 2013, **110**, 1187–1192.

28. A. P. Berke, L. Turner, H. C. Berg and E. Lauga, *Phys. Rev. Lett.*, 2008, **101**, 038102.

29. P. Denissenko, V. Kantsler, D. J. Smith and J. Kirkman-Brown, *Proc. Natl. Acad. Sci.*, 2012, **109**, 8007–8010.

30. A. Bukatin, P. Denissenko and V. Kantsler, *Sci. Rep.*, 2020, **10**, 1–8.

31. F. Yazdan Parast, M. K. O'Bryan and R. Nosrati, *Adv. Mater. Technol.*, 2022, 2101291.

32. R. Nosrati, M. Vollmer, L. Eamer, M. C. San Gabriel, K. Zeidan, A. Zini and D. Sinton, *Lab. Chip*, 2014, **14**, 1142–1150.

33. M. Yaghoobi, M. Azizi, A. Mokhtare and A. Abbaspourrad, *Lab. Chip*, 2021, **21**, 2791–2804.

34. V. Kantsler, J. Dunkel, M. Blayney and R. E. Goldstein, *Elife*, 2014, **3**, e02403.

35. M. Zaferani, S. H. Cheong and A. Abbaspourrad, *Proc. Natl. Acad. Sci.*, 2018, **115**, 8272–8277.

36. M. Zaferani, G. D. Palermo and A. Abbaspourrad, *Sci. Adv.*, 2019, **5**, eaav2111.

37. J. Romero-Aguirregomezcorta, R. Laguna-Barraza, R. Fernández-González, M. Štiavnická, F. Ward, J. Cloherty, D. McAuliffe, P. B. Larsen, A. M. Grabrucker and A. Gutiérrez-Adán, *Reproduction*, 2021, **161**, 343–352.

38. S. Sharma, M. A. Kabir and W. Asghar, *Analyst*, 2022, **147**, 1589–1597.

39. I. R. Sarbandi, A. Lesani, M. Moghimi Zand and R. Nosrati, *Sci. Rep.*, 2021, **11**, 18327.

40. S. Zeaei, M. Z. Targhi, I. Halvaei and R. Nosrati, *Lab. Chip*, 2023, **23**, 2241–2248.

41. M. Yaghoobi, M. Azizi, A. Mokhtare, F. Javi and A. Abbaspourrad, *Lab. Chip*, 2022, **22**, 1486–1497.

42. S. S. Suarez and A. A. Pacey, *Hum. Reprod. Update*, 2006, **12**, 23–37.

43. A. Olanrewaju, M. Beaugrand, M. Yafia and D. Juncker, *Lab. Chip*, 2018, **18**, 2323–2347.

44. C. Tung, F. Ardon, A. Roy, D. L. Koch, S. S. Suarez and M. Wu, *Phys. Rev. Lett.*, 2015, **114**, 108102.

45. E. Altshuler, G. Mino, C. Pérez-Penichet, L. Del Río, A. Lindner, A. Rousselet and E. Clément, *Soft Matter*, 2013, **9**, 1864–1870.

46. K. Cui and C. D. Matthews, *Nature*, 1993, **366**, 117–118.

47. R. A. P. Harrison, H. M. Dott and G. C. Foster, *J. Exp. Zool.*, 1982, **222**, 81–88.

48. J. J. Parrish, J. L. Susko-Parrish and N. L. First, *Biol. Reprod.*, 1989, **41**, 683–699.

682 49. A. N. Fatehi, M. M. Bevers, E. Schoevers, B. A. J. Roelen, B. Colenbrander and B. M.
683 Gadella, *J. Androl.*, 2006, **27**, 176–188.

684 50. Y. Xia and G. M. Whitesides, *Annu. Rev. Mater. Sci.*, 1998, **28**, 153–184.

685 51. W. H. Organization, *WHO laboratory manual for the examination and processing of human*
686 *semen*, World Health Organization, 2021.

687 52. A. Guidobaldi, Y. Jeyaram, I. Berdakin, V. V. Moshchalkov, C. A. Condat, V. I. Marconi, L.
688 Giojalas and A. V. Silhanek, *Phys. Rev. E*, 2014, **89**, 032720.

689 53. A. Bukatin, I. Kukhtevich, N. Stoop, J. Dunkel and V. Kantsler, *Proc. Natl. Acad. Sci.*, 2015,
690 **112**, 15904–15909.

691

692